A&A 583, A21 (2015)
DOI: 10.1051/0004-6361/201526046

Astronomy & Astrophysics
Special feature

Rosetta mission results pre-perihelion

Rosetta observations of solar wind interaction with the comet 67P/Churyumov-Gerasimenko

T. W. Broiles[1], J. L. Burch[1], G. Clark[2,3], C. Koenders[4], E. Behar[5,6], R. Goldstein[1], S. A. Fuselier[1,7], K. E. Mandt[1], P. Mokashi[1], and M. Samara[2]

[1] Space Science and Engineering Division, Southwest Research Institute (SwRI), 6220 Culebra Rd San Antonio, TX 78238, USA
e-mail: tbroiles@swri.edu
[2] Heliophysics Division, Goddard Space Flight Center, 8800 Greenbelt Road Greenbelt, MD 20771, USA
[3] Department of Physics and Astronomy, The Catholic University of America, 620 Michigan Ave NE, Washington, DC 20064, USA
[4] Institut für Geophysik und extraterrestrische Physik, Technische Universität Braunschweig, Mendelssohnstraße 3, 38106 Braunschweig, Germany
[5] Swedish Institute for Space Physics, PO Box 812, 981 28 Kiruna, Sweden
[6] Luleå University of Technology, Department of Computer Science, Electrical and Space Engineering, Rymdcampus 1, 981 28 Kiruna, Sweden
[7] The University of Texas at San Antonio, Department of Physics and Astronomy, 1 UTSA Circle, San Antonio, TX 78249, USA

Received 6 March 2015 / Accepted 20 May 2015

ABSTRACT

Context. The Rosetta spacecraft arrived at the comet 67P/Churyumov-Gerasimenko on August 6, 2014, which has made it possible to perform the first study of the solar wind interacting with the coma of a weakly outgassing comet.
Aims. It is shown that the solar wind experiences large deflections (>45°) in the weak coma. The average ion velocity slows from the mass loading of newborn cometary ions, which also slows the interplanetary magnetic field (IMF) relative to the solar wind ions and subsequently creates a Lorentz force in the frame of the solar wind. The Lorentz force in the solar wind frame accelerates ions in the opposite direction of cometary pickup ion flow, and is necessary to conserve momentum.
Methods. Data from the Ion and Electron Sensor are studied over several intervals of interest when significant solar wind deflection was observed. The deflections for protons and for He^{++} were compared with the flow of cometary pickup ions using the instrument's frame of reference. We then fit the data with a three-dimensional Maxwellian, and rotated the flow vectors into the Comet Sun Equatorial coordinate system, and compared the flow to the spacecraft's position and to the local IMF conditions.
Results. Our observations show that the solar wind may be deflected in excess of 45° from the anti-sunward direction. Furthermore, the deflections change direction on a variable timescale. Solar wind protons are consistently more deflected than the He^{++}. The deflections are not ordered by the spacecraft's position relative to the comet, but large changes in deflection are related to changes in the orthogonal IMF components.

Key words. solar wind – comets: general – plasmas – Sun: magnetic fields – methods: observational – methods: data analysis

1. Introduction

The interaction of the solar wind with the neutral gas that forms the coma of a comet is of great historical interest. In situ observations provide important insight into the impact that cometary neutral gas has on the solar wind, but have been limited to a few flybys of very active comets (Cravens & Gombosi 2004). The Rosetta mission provides a unique opportunity for long-term observation of the interaction of the solar wind with a weak comet for which the activity is gradually increasing as it approaches the Sun. These observations combined with theoretical simulations help us to better understand how the solar wind interacts with a comet. In the coma of a comet, neutral gas diffuses radially outward, and will eventually ionize through photoionization with sunlight or charge-exchange with the solar wind (Combi et al. 2005). The newborn cometary ions are initially slow (~1 km s^{-1}) compared to the solar wind (~400 km s^{-1}), which leads to a Lorentz force that accelerates the cometary ions orthogonal to the direction of solar wind flow, $\boldsymbol{v}_{SW}$, and interplanetary magnetic field (IMF), $\boldsymbol{B}_{IMF}$. Through this acceleration process, particles are "picked up", begin to gyrate around the IMF, and as more ions are created, a ring distribution forms around the solar wind in phase space (Coates et al. 1989; Coates 2004). Pickup ions increasingly mass load the solar wind, which causes deceleration through conservation of momentum (Biermann et al. 1967) and the excitation of wave activity (Wu & Davidson 1972; Szegö et al. 2000).

The neutral outgassing rate is very high when comets are near the Sun, and consequently, the neutral population remains large enough for substantial ion production far from the comet (>100 000 km). The large coma size of active comets ($Q_{Neutral} \simeq 1 \times 10^{29}$ mol s^{-1}) causes significant solar wind deceleration, which makes the formation of a diamagnetic cavity and bow shock possible (Biermann et al. 1967; Neubauer et al. 1986; Mendis et al. 1986). In contrast, ion production at inactive comets ($Q_{Neutral} \simeq 5 \times 10^{26}$ mol s^{-1}) is weaker because of the lower neutral production rate and the reduced flux of ionizing light and solar wind farther from the Sun. Consequently, mass loading of the solar wind only becomes significant within 1000 km from inactive comets, and does not cause significant deceleration (Rubin et al. 2014). The scale size of a weak comet's ion coma is small compared to the cycloidal motion of most

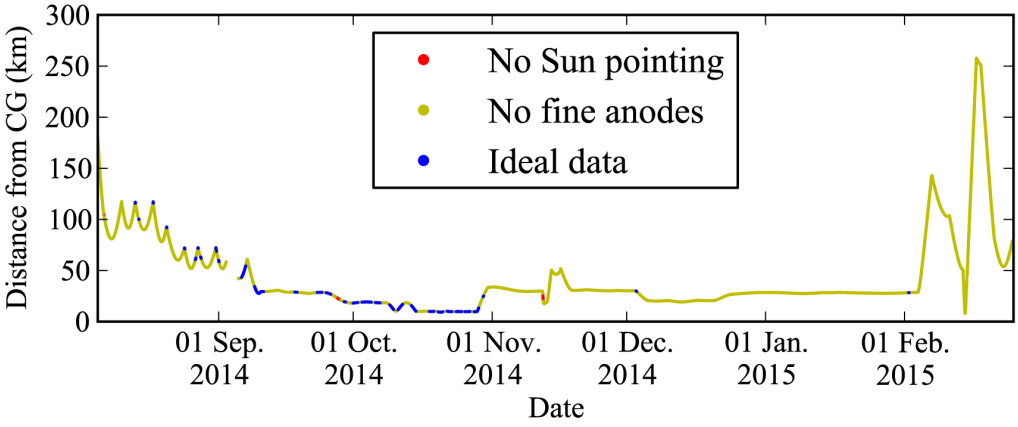

Fig. 1. Distance of Rosetta from 67P vs. time. Intervals when the Sun was out of the IES field of view are red, intervals when IES had poor angular resolution of the solar wind are yellow, intervals with high angular resolution solar wind observations are blue.

cometary pickup ions, and as a result, kinetic effects become important (Bagdonat & Motschmann 2002). Hybrid and multi-fluid magnetohydrodynamic (MHD) simulations of weak ion comas show that there is insufficient time for a pickup ring distribution to form, and is limited to a low energy pickup "tail" that flows away from the comet in the $-\boldsymbol{v}_{SW} \times \boldsymbol{B}_{IMF}$ direction (Bagdonat & Motschmann 2002; Rubin et al. 2014; Koenders et al. 2015). These models also show that the solar wind experiences a Lorentz force in the opposite direction to the pickup ions that is necessary to conserve momentum and energy.

Observations of the interaction between the solar wind and cometary ionospheres were studied previously at the comets Giaccobini-Zinner (Sanderson et al. 1986), Halley (Mukai et al. 1986; Johnstone 1990; Neubauer 1990), Grigg-Skjellerup (Johnstone et al. 1993), Borrelly (Young et al. 2004; Richter et al. 2011). With exception to Giaccobini-Zinner, each spacecraft passed through a cometary bow shock, observed gradual deceleration of the solar wind with simultaneous deflection away from the Sun-comet line, and in the case of Giotto at 1P/Halley, a diamagnetic cavity was observed. However, these comets were much more active than 67P/Churyumov-Gerasimenko (67P), and were observed around 1 AU (Gulkis et al. 2015; Bieler et al. 2015). Conditions closer to those at 67P were evaluated by the Active Magnetospheric Particle Tracer Explorers (AMPTE), which simulated the ion coma of a weakly outgassing comet by creating a neutral coma of lithium or barium around their spacecraft (Valenzuela et al. 1986). Chapman & Dunlop (1986) found that the solar wind was deflected because momentum was conserved between the solar wind and newly accelerated pickup ions.

In this work, we show the first detailed observations from the Rosetta spacecraft at 67P of the solar wind interacting with the weak ion coma of a comet far from the Sun (~3 AU). In contrast to previous cometary encounters, we expect the solar wind to have undergone little deceleration, but it may be still heavily deflected through the conservation of momentum with freshly accelerated cometary pickup ions.

2. Results

2.1. Instrumentation

The Ion and Electron Sensor (IES) is one of two plasma spectrometers onboard Rosetta that measures ions and electrons with energies per charge between of 4.3 eV/q to 18 keV/q, and a $\Delta E/E$ of 8%. The instrument has a 360° × 90° field of view with an angular resolution of 5° × 6° for ions and 22.5° × 6° for electrons (Burch et al. 2007). Measurements are made at a variable cadence, between 128 and 1024 s. However, it is impossible to simultaneously meet the above mentioned energy, angular, and time resolution within telemetry constraints. These constraints necessitate the use of measurement modes that collapse adjacent measurements in energy, elevation, or time to focus on specific science goals.

For example, the ion portion of IES has 7 coarse (45°) and 9 fine (5°) anodes. In order to resolve the three-dimensional velocity distribution function (VDF) of solar wind ions, IES must be oriented such that the fine anodes have good pointing toward the Sun, and IES must use a mode that returns all data from those anodes. When IES uses a mode that collapses data from the fine anodes, the instrument effectively has eight 45° wide azimuthal look directions. Consequently, modes without the fine anodes limit our analysis of the solar wind VDF.

2.2. Observations

Rosetta arrived at 67P on August 6, 2014. Since that time IES has made near continuous observation of the solar wind, with the exception of rare periods when the Sun was outside of the IES field of view or behind a spacecraft blockage. However, as mentioned in Sect. 2.1, IES is also constrained by Rosetta's pointing and telemetry requirements.

Figure 1 shows the distance of Rosetta from the comet between August 6, 2014, and February 26, 2015. Measurements are colored to qualify their use for study of solar wind deflection; red data when the Sun was outside of the IES field of view, yellow data when the Sun was outside of the field of view of the fine anodes or the instrument was using a mode that had poor angular resolution, or blue data when the Sun was in the field of view of the fine anodes and the instrument was in a mode that had high angular resolution. We had many days of ideal solar wind measurements in October and a few in January, when Rosetta was between 10−30 km from the comet. This work focuses on intervals near the comet (<50 km) when ideal solar wind measurements were made.

Figure 2 shows the ion flux over the entire day of October 20, 2014. Panel a shows the flux at each energy/charge versus time, panel b shows the flux at each elevation versus time, and panel c shows the flux at each azimuth versus time. White dashed lines in panels b and c show the position of the Sun over time in

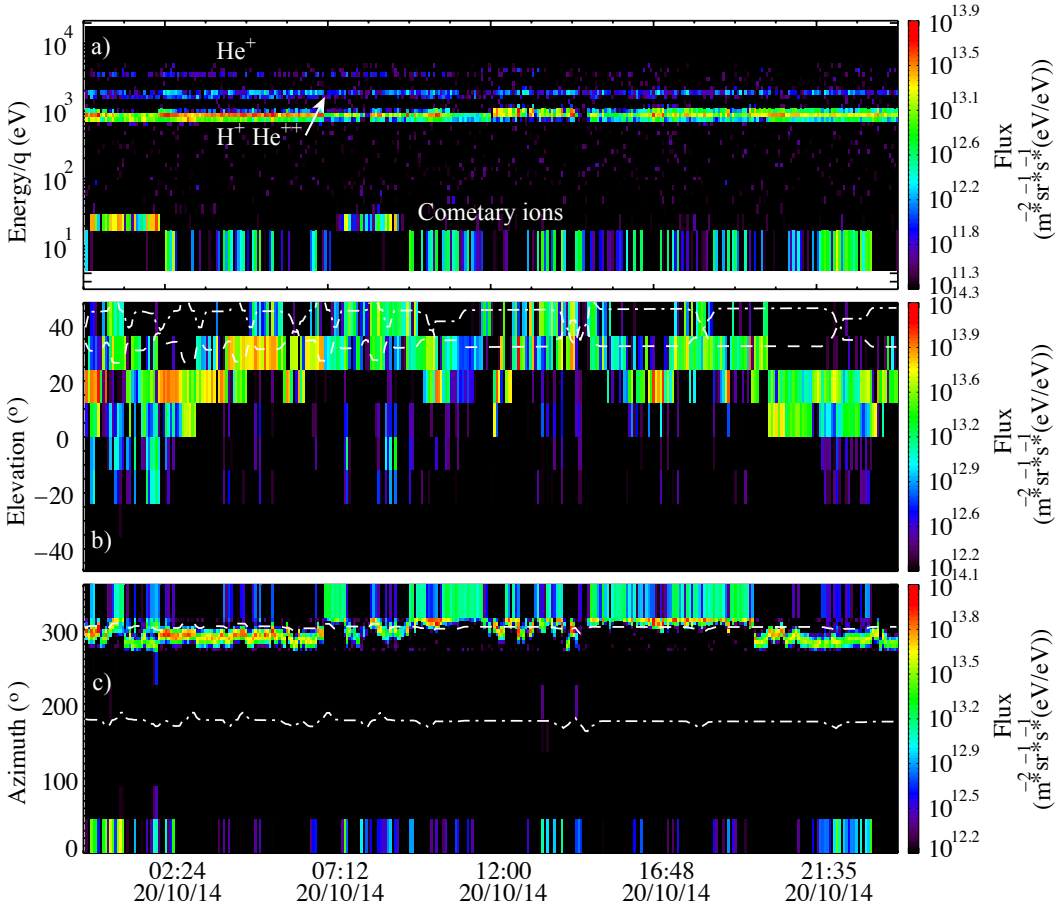

Fig. 2. IES data from the ion instrument on October 20, 2014. **a)** Energy/q versus time; **b)** elevation angle versus time; and **c)** azimuth angle versus time. White dashed lines in panels **b)** and **c)** show the Sun's elevation and azimuth in the IES reference frame. White dashed-dotted lines in panels **b)** and **c)** show 67P's elevation and azimuth in the IES reference frame.

the field of view of IES, while white dashed-dotted lines show the position of 67P.

Four clear signals are shown in Fig. 2a. The lowest energy/q signal are newly formed cometary ions (Nilsson et al. 2015). The increases in energy, at ~01:00 and ~08:00, are caused by an enhanced negative spacecraft potential accelerating the cometary ions. The ions observed at 800 and 1600 eV/q are solar wind protons and He^{++}, respectively. We note that there is very little change to the solar wind speed throughout the day. The faint signal at 3.5 keV/q is likely He^{+}. This ion is created by charge exchange of solar wind He^{++} with cometary neutrals (Shelley et al. 1987; Fuselier et al. 1991).

Figures 2b and c both show that the solar wind is significantly deflected near the comet. The signal from all 4 ion species are shown in panels b and c; all four species appear between −20° and 50° in elevation, but in azimuth the solar wind ions are distinct and mostly observed in the fine anodes (270°−315°). The clearest example of strong solar wind deflection occurs after 19:00, when the majority of the solar wind flux occurs at azimuths and elevations that are more than 20° from the anti-sunward line. Solar wind deflections are also highly variable. Between 11:00 and 13:00, the solar wind periodically oscillates across the azimuth of the Sun every 20 min, but at other times throughout the day the solar wind remained consistently deflected for several hours or more.

We now choose a time period during which the spacecraft orientation and the solar wind deflection do not change significantly and when the He^{+} signal was intense enough to evaluate the degree of deflection of the solar wind during these time periods. Figure 3 shows time averaged flux from October 20, 2014, between 03:30 and 04:10, for all energies/q in each anode summed over elevation. The azimuth of the Sun is marked with a black diamond. The radial direction relative to the Sun is shown with a horizontal dotted line and tick marks show the relative energy per charge along this line. We also calculate velocity scales for all 4 species along the abscissa and ordinate of the figure. We note that prior to arrival at the comet, IES data showed the undisturbed solar wind rarely exceeds 5−10° from the anti-sunward direction. However, the solar wind protons in Fig. 3 are deflected in azimuth alone by almost 20°. We also note that the heavier He^{++} are only deflected about 8° or 9° and He^{+} is deflected similarly to that of the He^{++}.

The Ion and Electron Sensor did not observe significant pickup ion acceleration on October 20, 2014. However, pickup ions were observed on January 23, 2015; Fig. 4 shows the time averaged flux, between 19:00 and 20:00 on this day, in the same format as Fig. 3. A precise estimate of the solar wind H^{+} deflection is not possible in this example because it extends more than 45° and exceeds the azimuthal extent of IES's fine anodes. As in Fig. 3, the He^{++} and He^{+} particles are deflected less than the protons (~30°), and remain within IES's fine anodes. If the ratio of deflection between H^{+} and He^{++} is similar to what was observed in Fig. 3, then we can estimate the solar wind proton deflection to be twice that of the He^{++} (~60°). In this case, the accelerated cometary pickup ions are moving at an angle of less than 45° from the azimuth of the Sun, but still orthogonal to the flow of

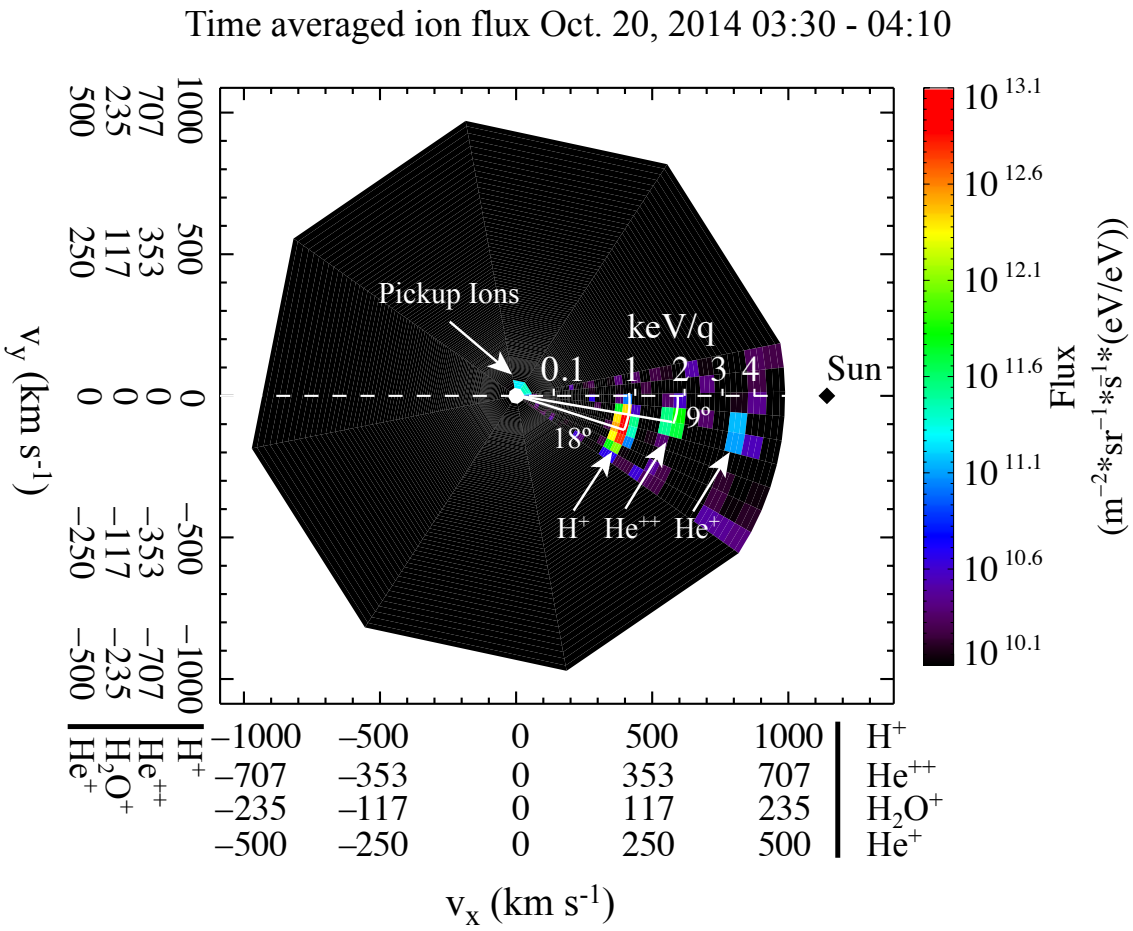

Fig. 3. Time averaged IES data summed over all elevations from the ion instrument on October 20, 2014, between 03:30 and 04:10. Solar wind protons, He^{++}, and He^{+} are all moving at approximately the same speed, but separated by our measurements into energy per charge. We show velocity scales for solar wind protons, He^{++}, H_2O^{+}, and He^{+} along the abscissa and ordinate. For example, the He^{++} have 4 times the mass (and energy) and twice the charge of protons. As a result, IES observes solar wind He^{++} at twice the energy per charge of protons. The black diamond shows the azimuth of the Sun in the IES field of view.

solar wind protons. In addition, the pickup ions are deflected to the opposite side of the spacecraft-Sun line as the solar wind.

2.3. Fitting analysis of solar wind data

In order to precisely characterize the solar wind behavior around the comet, IES data was fit to a Maxwellian using the Levenberg-Marquardt algorithm (Marquardt 1963). When solar wind data with high spatial resolution was available, the measured distribution function, $f(\boldsymbol{v})$, was fit with Eq. (1) to compute the density, n, velocity, $\boldsymbol{v}_{\rm SW}$, and temperature, T, of the solar wind protons and He^{++}:

$$f(\boldsymbol{v}) = n\left(\frac{m}{2\pi kT}\right)^{\frac{3}{2}} \exp\left(\frac{-m(\boldsymbol{v}-\boldsymbol{v}_{\rm SW})^2}{2kT}\right). \quad (1)$$

Figure 5 illustrates the flow of solar wind at the position of the spacecraft throughout October 20, 2014. Panel a shows the flow in the Cometocentric Solar Equatorial (CSEQ) coordinate system x–z plane, while panel b shows the flow in the y–z plane. In the CSEQ frame, x points toward the Sun, z is aligned with the solar rotation axis, and y is orthogonal to x and z. The spacecraft position is marked with blue dots, 67P is marked with a black dot, and the flow of solar wind protons is shown with black arrows. The deflection of the solar wind is not ordered by the spacecraft's position relative to the comet.

Figure 6 shows a time series analysis of our fitting results in the CSEQ coordinate system, over the entire day of October 20, 2014. Red data is used for the fitting results for He^{++} when available. Panel a shows solar wind speed, $|\boldsymbol{v}_{\rm SW}|$, panel b shows the solar wind elevation angle $\theta = \arcsin\left(\frac{v_z}{|\boldsymbol{v}_{\rm SW}|}\right)$, panel c shows the solar wind azimuthal angle $\phi = \arctan 2\left(\frac{v_y}{v_x}\right)$, and panel d shows the magnetic field components (Bx: black data, By: red data, and Bz: blue data) in CSEQ obtained by RPC-MAG (Glassmeier et al. 2007). The spacecraft residual magnetic field is unknown, which also means that the total magnetic field strength and direction are unknown. Consequently, this study uses relative changes in the components of the magnetic field data. We also note that the uncertainty in our fitting analysis is estimated to be on the order of the IES resolution (~5°).

Our fitting analysis confirms that solar wind H^{+} is deflected more than 25° from the comet-Sun line. Moreover, we note that solar wind He^{++} is consistently less deflected than that of the protons. Vertical dashed lines mark four changes in the solar wind deflection that relate to changes in the magnetic field. Around 01:00, the azimuthal deflection of the solar wind reverses from negative to positive and then back to negative 30 min later, while a similar behavior is observed in the IMF Bx (black) and Bz (blue) components. Again at 07:00, the azimuthal angle reverses from negative to positive in conjunction with a positive change in Bx (black) and Bz (blue). At 19:30, the solar wind

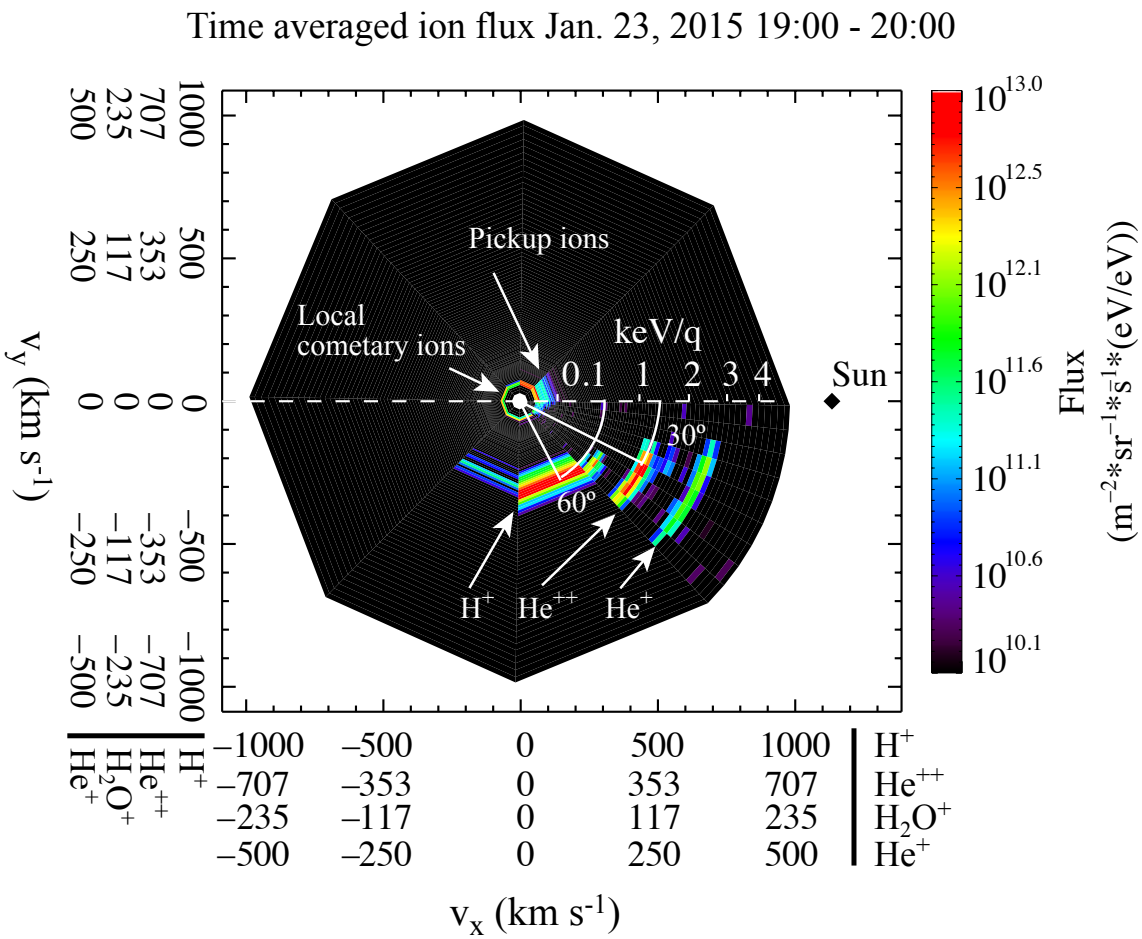

Fig. 4. Time averaged IES data from the ion instrument on January 23, 2015, between 19:00 and 20:00 in the same style as Fig. 3.

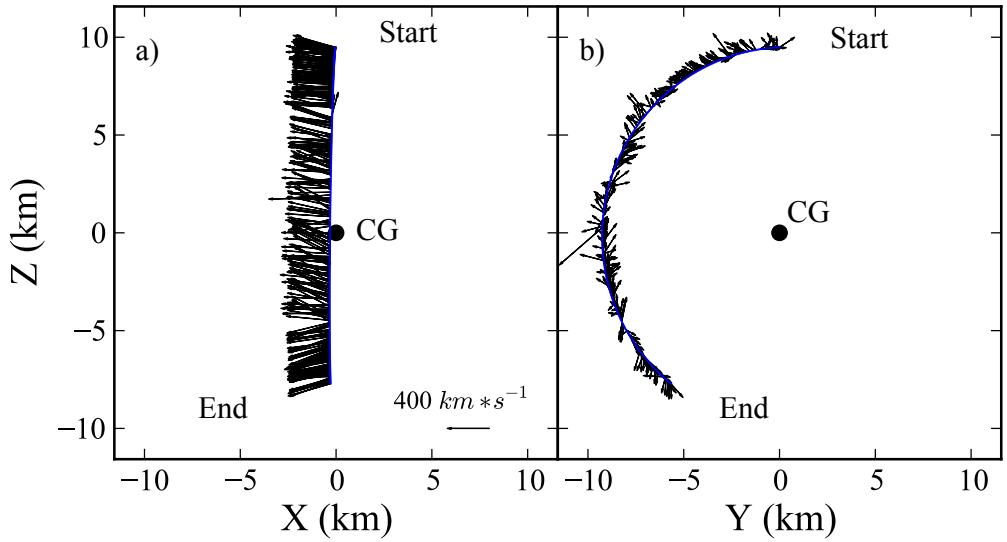

Fig. 5. Observed flow of the solar wind on October 20, 2014, by Rosetta. Panels **a)** and **b)** respectively show the *x*–*z* and *y*–*z* planes in the CSEQ coordinate system. Black dot: 67P, blue curve: Rosetta's flight path, black arrows: solar wind flow.

elevation angle reverses from positive to negative at the same time as By (red) changes positively and Bx (black) changes negatively. It was carefully checked that the state of the spacecraft, e.g., spacecraft currents, do not have a significant impact on the measured magnetic field at these times. Thus, the observed changes in the magnetic field are present in the IMF and not caused by the spacecraft. In synopsis, abrupt changes in solar wind deflection often occur with simultaneous changes in the orthogonal magnetic field components.

3. Summary and discussion

This study uses data from Rosetta's Ion and Electron Sensor to make the first detailed observations of solar wind interacting

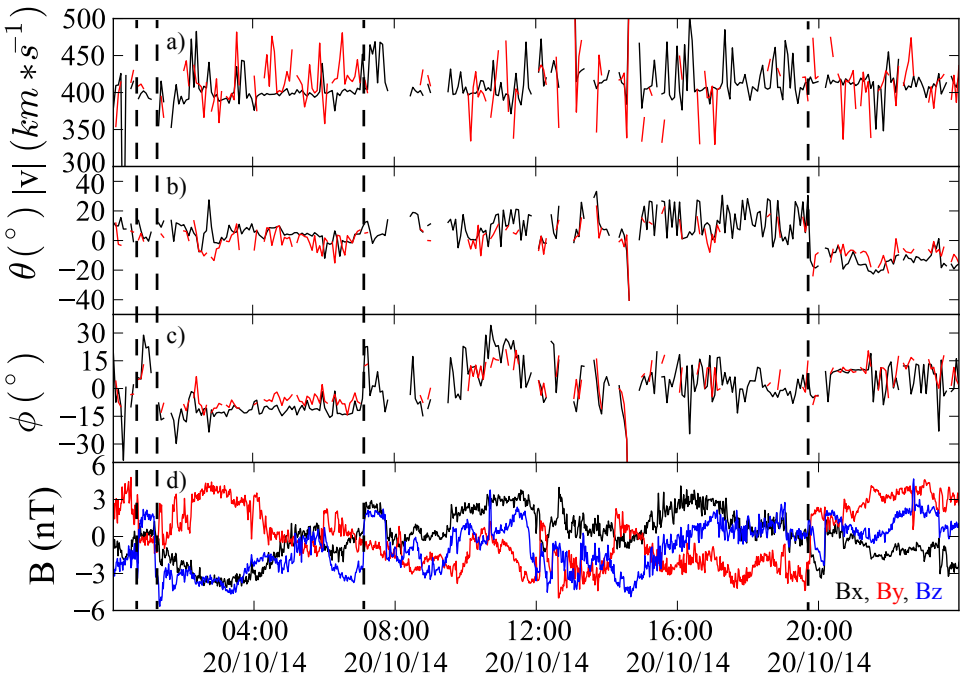

Fig. 6. Fitting results of IES data in CSEQ coordinates from October 20, 2014, for protons (black) and He^{++} (red). *From top to bottom*: **a)** speed; **b)** elevation angle; **c)** azimuthal angle; **d)** magnetic field components Bx (black), By (red), Bz (blue).

Table 1. A summary of our analysis to determine coma ion densities from the deflection of the solar wind.

Date	n_{SW} (cm^{-3})	$v_{SW\perp}$ (km s^{-1})	$v_{CI\perp}$ (km s^{-1})	n_{CI} (cm^{-3})
2014-Oct.-20 03:30-04:10	0.6	sin(18°)*390 = 120	sin(90°−18°)*10 = 9.5	0.4
2015-Jan.-23 19:00-20:00	1.8	sin(60°)*314 = 272	sin(90°−60°)*18 = 9	3.0

Notes. From *left* to *right* the columns are: date of analysis, solar wind density, solar wind velocity perpendicular to the anti-sunward direction, cometary ion velocity perpendicular to the anti-sunward direction, and coma ion density.

with a weakly outgassing comet. We find that the solar wind is not appreciably slowed by the coma, but is deflected significantly. Furthermore, the solar wind protons are deflected greater than the solar wind He^{++}. Pickup ions are accelerated in a direction perpendicular to the flow of solar wind protons, and on the opposing side of the spacecraft-Sun line. Moreover, the solar wind does not consistently deflect around the comet as observed previously at comets with bow shocks (Mukai et al. 1986; Johnstone et al. 1993; Young et al. 2004). However, we find that reversals in the solar wind deflection relate to changes in the orthogonal magnetic field components. These results show clear evidence of solar wind deflection caused by momentum transfer with the newly accelerated cometary ions, and are in good agreement with observations made at a simulated comet and theoretical predictions (Chapman & Dunlop 1986; Bagdonat & Motschmann 2002; Rubin et al. 2014; Koenders et al. 2015).

Figures 3 and 4 show that solar wind protons are more strongly deflected than the solar wind He^{++} or He^{+}. In the case of Fig. 3, the proton deflection was larger by a factor of 2, which is proportional to the charge/mass (q/m) ratio between the two species and is further evidence that the solar wind deflection is caused by a Lorentz force. Particle acceleration, $\boldsymbol{a}$, from a Lorentz force is proportional to q/m (i.e., $\boldsymbol{a} = -q(\boldsymbol{v} \times \boldsymbol{B})/m$). We suggest that He^{+} deflects similarly to He^{++} because the deflections largely occur before charge exchange. Deflection is a cumulative effect that steadily increases as newborn cometary ions are added upstream, while charge exchange is more likely to occur near the comet, where neutral densities are larger. We also comment on the increased magnitude of the deflections observed in Fig. 4; these observations were made in late January, when the comet was much closer to the Sun. We speculate that the reduced distance from the Sun has resulted in a larger, denser ion coma that more efficiently deflects the solar wind.

Figure 6 shows that changes in solar wind deflection relate to changes in the orthogonal magnetic field components. We think that the reversals in solar wind deflection are caused by changes in sign of the orthogonal magnetic field components, which subsequently reverse the direction of the Lorentz forces experienced by the solar wind and pickup ions. We suggest that this could be a useful in-flight analysis tool for the calibration of magnetometers.

Given that the solar wind is deflecting through a momentum transfer process, it is possible to speculate on the density of the ion coma necessary to cause the observed solar wind deflection. We use Figs. 3 and 4 as cases studies for this analysis. Equation (2) shows the balance in momentum between the solar wind and cometary ions, assuming the momentum of He^{++} and He^{+} is negligible. The relationship is defined by the solar wind number density, n_{SW}, proton mass, m_{SW}, the flow of solar wind perpendicular to the anti-sunward line, $v_{SW\perp}$, coma ion density, n_{CI}, cometary ion mass, m_{CI}, and the flow of cometary ions perpendicular to the anti-sunward line, $v_{CI\perp}$. This equation

is rearranged into the form shown in Eq. (3) to solve for the average coma ion density encountered by the solar wind upstream of the spacecraft:

$$n_{\rm SW} * m_p * v_{\rm SW\perp} = n_{\rm CI} * m_{\rm CI} * v_{\rm CI\perp} \quad (2)$$

$$n_{\rm CI} = \frac{n_{\rm SW} * m_p * v_{\rm SW\perp}}{m_{\rm CI} * v_{\rm CI\perp}}. \quad (3)$$

The solar wind and cometary ion masses are assumed constant at the mass of protons and water, respectively. We also assume that the flow of cometary pickup ions remains orthogonal to the flow of the solar wind based on results in Figs. 3 and 4. The magnitude of $v_{\rm CI\perp}$ is estimated from the peak of the pickup ion distribution in Figs. 3 and 4. Solar wind densities are calculated with our fitting analysis. Table 1 summarizes our results, and shows that the cometary pickup ions can cause significant deflection of the solar wind when their densities are approximately equal. We note that our cometary ion densities are in reasonable agreement with those predicted by Fuselier et al. (2015).

Acknowledgements. The work on IES was supported, in part, by the US National Aeronautics and Space Administration through contract #1345493 with the Jet Propulsion Laboratory, California Institute of Technology. We thank the teams at Imperial College London and ESA who have been responsible for the operation of IES. The work on RPC-MAG was financially supported by the German Ministerium für Wirtschaft und Energie and the Deutsches Zentrum für Luft- und Raumfahrt under contract 50QP 1401. We acknowledge the staff of CDDP and IC for the use of AMDA and the RPC Quicklook database (provided by a collaboration between the Centre de Données de la Physique des Plasmas, supported by CNRS, CNES, Observatoire de Paris and Université Paul Sabatier, Toulouse and Imperial College London, supported by the UK Science and Technology Facilities Council).

References

Bagdonat, T., & Motschmann, U. 2002, Earth, Moon, and Planets, 90, 305
Bieler, A., Altwegg, K., Balsiger, H., et al. 2015, A&A, 583, A7
Biermann, L., Brosowski, B., & Schmidt, H. U. 1967, Sol. Phys., 1, 254
Burch, J. L., Goldstein, R., Cravens, T. E., et al. 2007, Space Sci. Rev., 128, 697
Chapman, S. C., & Dunlop, M. W. 1986, J. Geophys. Res.: Space Phys., 91, 8051
Coates, A. J. 2004, Adv. Space Res., 33, 1977
Coates, A. J., Johnstone, A. D., Wilken, B., Jockers, K., & Glassmeier, K.-H. 1989, J. Geophys. Res.: Space Phys., 94, 9983
Combi, M. R., Harris, W. M., & Smyth, W. H. 2005, Gas Dynamics and Kinetics in the Cometary Coma: Theory and Observations
Cravens, T., & Gombosi, T. 2004, Adv. Space Res., 33, 1968
Fuselier, S. A., Shelley, E. G., Goldstein, B. E., et al. 1991, ApJ, 379, 734
Fuselier, S. A., Altwegg, K., Balsiger, H., et al. 2015, A&A, 583, A2
Glassmeier, K.-H., Richter, I., Diedrich, A., et al. 2007, Space Sci. Rev., 128, 649
Gulkis, S., Allen, M., Allmen, P. V., et al. 2015, Science, 347, 0709
Johnstone, A. D. 1990, in Comet Halley: Investigations, Results, Interpretations, Organization, Plasma, Gas, 1, 57
Johnstone, A. D., Coates, A. J., Huddleston, D. E., et al. 1993, A&A, 273, L1
Koenders, C., Glassmeier, K. H., Richter, I., Ranocha, H., & Motschmann, U. 2015, Planet. Space Sci., 105, 105
Marquardt, D. 1963, J. Soc. Industrial Appl. Math., 11, 431
Mendis, D. A., Smith, E. J., Tsurutani, B. T., et al. 1986, Geophys. Res. Lett., 13, 239
Mukai, T., Miyake, W., Terasawa, T., Kitayama, M., & Hirao, K. 1986, Nature, 321, 299
Neubauer, F. M. 1990, in Comet Halley: Investigations, Results, Interpretations, Organization, Plasma, Gas, 1, 79
Neubauer, F. M., Glassmeier, K. H., Pohl, M., et al. 1986, Nature, 321, 352
Nilsson, H., Stenberg Wieser, G., Behar, E., et al. 2015, Science, 347, 0571
Richter, I., Koenders, C., Glassmeier, K., Tsurutani, B., & Goldstein, R. 2011, Planet. Space Sci., 59, 691
Rubin, M., Koenders, C., Altwegg, K., et al. 2014, Icarus, 242, 38
Sanderson, T. R., Wenzel, K.-P., Daly, P., et al. 1986, Geophys. Res. Lett., 13, 411
Shelley, E. G., Fuselier, S. A., Balsiger, H., et al. 1987, in Exploration of Halley's Comet, eds. P. D. M. Grewing, P. D. F. Praderie, & D. R. Reinhard (Berlin, Heidelberg: Springer), 304
Szegö, K., Glassmeier, K.-H., Bingham, R., et al. 2000, Space Sci. Rev., 94, 429
Valenzuela, A., Haerendel, G., Föppl, H., et al. 1986, Nature, 320, 700
Wu, C. S., & Davidson, R. C. 1972, J. Geophys. Res., 77, 5399
Young, D., Crary, F., Nordholt, J., et al. 2004, Icarus, 167, 80